Electrochimica Acta 569 (2026) 148894

Contents lists available at ScienceDirect

Electrochimica Acta

journal homepage: www.journals.elsevier.com/electrochimica-acta

Sustainable iodine activation via ultrasound-assisted contact-electro-chemistry

Xinyi Huo [a,b,1], Han Qian [b,c,1], Ning Wu [b,1], Zeyang Yu [b,c], Bing Sun [a,*], Zhong Lin Wang [b,*], Di Wei [b,*]

[a] School of Science, China University of Geosciences, Beijing 100083, China
[b] Beijing Institute of Nanoenergy and Nanosystems, Chinese Academy of Sciences, Beijing 101400, China
[c] School of Nanoscience and Engineering, University of Chinese Academy of Sciences, Beijing 100049, China

ARTICLE INFO

Keywords:
Contact-electro-chemistry (CE-chemistry)
Marine biomass
Iodine activation
Electrical double layer (EDL)
Charge transfer

ABSTRACT

Marine biomass represents an abundant, low-cost and carbon-neutral resource for sustainable chemical production, yet the extraction and activation of kelp-derived iodine typically rely on added oxidants and harsh processing conditions, leading to high energy input, poor selectivity and problematic by-products. Developing green and efficient routes for iodine recovery from marine resources therefore remains a challenge. Here we propose an oxidant-free contact-electro-chemistry (CE-Chemistry) strategy with the potential to enable extraction and conversion from kelp under ambient conditions, with strong tolerance to pH variation and ionic interference. Iodide released from kelp through pyrolysis and boiling may be directionally oxidized via an ultrasound-assisted process, in which interfacial electron transfer and in situ •OH generation cooperatively drive iodine activation. This approach achieves a triiodide formation yield of 107.45 μmol g^{-1} h^{-1}. The resulting iodine complex, formulated with poly(vinylpyrrolidone), functions as an iodophor disinfectant and delivers a 6-log (99.9999%) reduction of *Staphylococcus aureus* and *Escherichia coli*. Through systematic interrogation of the liquid-solid (L-S) interfacial microenvironment, the dynamic regulation of the electrical double layers (EDLs) is revealed as a governing factor in CE-Chemistry reaction efficiency. Beyond establishing a green and low-cost route to high-performance iodophor disinfectants, CE-Chemistry is, for the first time, extended to marine biomass valorization, providing a general framework for EDL-mediated interfacial reaction and advancing the sustainable, high-value utilization of marine resources.

1. Introduction

Marine biomass, as an abundant, low-cost, and carbon-neutral renewable resource, has emerged as a pivotal candidate for sustainable biorefinery [1,2]. Among them, kelp-represented marine biomass has garnered increasing attention due to its rich content of high-value elements such as iodine [2,3]. The extraction and utilization of iodine from kelp hold significant practical value for the development of iodine-based products and the high-value valorization of marine biomass resources [4]. However, conventional kelp iodine extraction and conversion routes face substantial challenges. These processes typically depend on chemical oxidants such as hydrogen peroxide or chlorine and require harsh conditions, including elevated temperature and pressure, to oxidize iodide (I^-) into active iodine species (I_2, I_3^-) [5–7]. Such approaches entail high energy consumption, poor selectivity, environmental pollution, and the generation of toxic by-products, which complicate downstream purification [8–11]. Moreover, their strong sensitivity to solution pH and ionic composition results in unstable yields, limiting scalability [1,12–14]. The intrinsic recalcitrance of biomass structures, together with reliance on external oxidants, further intensifies the trade-offs between efficiency, sustainability and cost in conventional technologies.

Contact-electro-chemistry (CE-Chemistry) is an emerging strategy for regulating interfacial charge transfer, rooted in contact electrification (CE) that has garnered growing attention for enabling green and energy-efficient chemical transformations [15–18]. Driven by mechanically induced contact and separation, this approach promotes interfacial charge transfer, leading to radical generation and the establishment

* Corresponding authors.
E-mail addresses: sunbing@cugb.edu.cn (B. Sun), zlwang@binn.cas.cn (Z.L. Wang), weidi@binn.cas.cn (D. Wei).
[1] These authors contributed equally: Xinyi Huo, Han Qian, Ning Wu.

https://doi.org/10.1016/j.electacta.2026.148894
Received 4 February 2026; Received in revised form 3 April 2026; Accepted 18 April 2026
Available online 21 April 2026
0013-4686/© 2026 Elsevier Ltd. All rights are reserved, including those for text and data mining, AI training, and similar technologies.

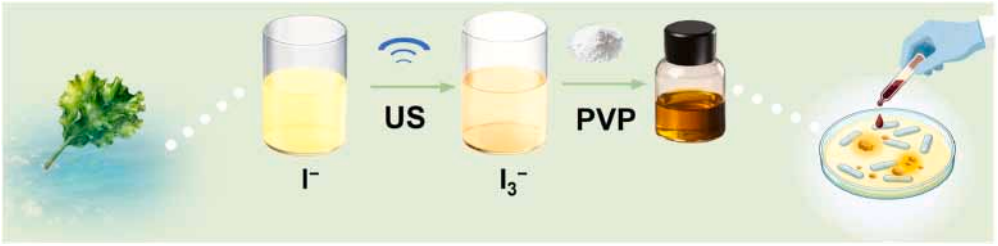


Fig. 1. Schematic diagram of the experimental procedure.

of triboelectric fields, thereby eliminating the need for precious-metal catalysts, including added chemical oxidants or reductants, as well as extreme reaction conditions [19–21]. As early as the 1980s, El-Kazzaz and Rose-Innes [22] investigated liquid-solid (L-S) CE involving liquid metals and solid insulators, although the underlying mechanisms were not fully clarified at that time. In the 1990s, Matsui, Yatsuka, and co-workers [23] systematically examined CE between water droplets and insulating surfaces (e.g., Teflon and polymer resins), revealing that water droplets consistently acquire positive charges during sliding contact with these materials. Wang and co-workers [24] investigated L-S CE and the thermal decay of surface charges, demonstrating their coexistence and proposing a two-step charge-transfer model that confirmed electrical double layer (EDL) formation. They further identified electron transfer as the dominant mechanism in the initial charging process, laying the foundation for L-S triboelectric nanogenerators (TENGs) [25]. Wei and co-workers [26] first demonstrated that organic solvents, particularly dimethyl sulfoxide (DMSO), can effectively support electrochemical polymerization. Building on this insight, subsequent studies revealed that, in contrast to aqueous systems where EDL screening severely hinders charge transfer, the use of organic solvents such as DMSO can significantly alleviate electrostatic screening, thereby enhancing charge-transfer efficiency and reaction selectivity in CE-Chemistry [27,28]. To date, CE-Chemistry has shown considerable promise across a range of applications, including environmental remediation, energy conversion, fine chemical synthesis, and resource recycling, underscoring its broad capability to activate small molecules and drive complex chemical transformations under ambient conditions [5, 29–31]. For example, Zhao et al. [10] demonstrated that ultrasonic mechanical excitation can promote interfacial electron transfer at L-S interfaces, enabling hydrogen peroxide synthesis with yield reaching 313 μmol g^{-1} h^{-1}. Wang et al. [32] harnessed contact-induced reactive oxygen species for the efficient degradation of methyl orange, illustrating the applicability of CE-Chemistry to pollutant remediation. Wei et al. [33] further established that redox selectivity in CE-Chemistry is governed by the standard electrode potential (SEP) of the participating species, identifying a critical threshold that determines the dominance of oxidative or reductive pathways. Wei et al. [34] developed a low-cost, tunable fluorinated silicon powder (F-Si) with controllable surface functionalization via fluorinated alkyl chains, which markedly enhances pollutant degradation efficiency and, for the first time, enables noble-metal-free reaction of I^- to I_3^- oxidation. These results establish a sustainable materials design framework for CE-Chemistry and, importantly, provide direct evidence that CE-Chemistry is intrinsically an interfacial phenomenon, in which chemical reactions are triggered by intense electric fields localized at the outermost L-S interface rather than by bulk processes. Complementing this materials-based insight, Wang and co-workers [35] employed a customized liquid microjunction surface sampling probe (LMJ-SSP) to directly observe reproducible peptide oxidation. By systematically correlating oxidation extent with droplet evaporation time, drying frequency, and solid surface properties, they demonstrated that interfacial conditions critically govern CE-Chemistry-mediated reactions. In addition, Wei and Wang et al. [36–38] extended the CE-Chemistry mechanism to the field of chemiluminescence through in-depth insights. Together, these studies highlight the central role of interfacial electric fields and underscore the necessity of precise interface control for steering chemical outcomes in CE-Chemistry. They found that the increase in luminescence intensity was directly related to the improved chemiluminescent reactivity, providing new insights into the interplay of charge polarity, electron transfer, and reaction efficiency in CE-Chemistry. They also studied metal-free, low-cost contact-electro-luminescence (CEL), where active oxygen oxidizes luminol through contact electrification between dielectric materials and deionized water. This allows for controllable luminescence, facilitates mechanism research, and provides possibilities for specific detection in various fields. Despite these advances, existing studies have predominantly emphasized electron transfer and radical generation, while the decisive role of the local L-S interfacial microenvironment, encompassing pH, triboelectric field strength, and the spatial distribution of cations and anions, has received comparatively little attention [19,29,39]. In particular, how dynamic regulation of EDL modulates reaction kinetics and efficiency in CE-Chemistry remains poorly understood.

This study lays a foundation for developing a CE-Chemistry-based strategy for the efficient extraction and conversion of iodine from kelp, establishing a green, mild activation pathway free of external chemical oxidants (Fig. 1). The approach achieves an iodine formation yield of 107.45 μmol g^{-1} h^{-1} via ultrasound-assisted CE-Chemistry, and the resulting iodophor disinfectant exhibits excellent antibacterial activity, with a 99.9999% reduction rate against both Staphylococcus aureus and *Escherichia coli*. Mechanistically, this work reveals that reaction efficiency is controlled by the dynamic regulation of the electrical double layer (EDL), directly correlating EDL structure with interfacial radical chemistry. Compared with traditional iodine oxidation methods, this strategy avoids toxic oxidants and secondary pollution, operates under ambient conditions with only mechanical stimulation, and shows strong resistance to pH changes and ionic interference. These results not only provide a sustainable, cost-effective route for high-performance iodine disinfectants and expand the application of CE-Chemistry to marine biomass valorization, but also establish a general mechanism framework for EDL-mediated interfacial reactions, offering a new paradigm for the high-value, sustainable utilization of marine resources.

2. Experimental

2.1. Materials

Fluorinated ethylene propylene (FEP), polytetrafluoroethylene (PTFE), polyvinylidene fluoride (PVDF) and polyethylene (PE) powder were supplied by Dupont.

2.2. Chemical reagents

potassium iodide (SSKI oral solution), Iodine (I_2), Tert-butanol (98.0%), silver nitrate ($AgNO_3$), EDTA-2Na, p-benzoquinone (99.5%) were purchased from Sinopharm Chemical Reagent Co. Ltd. 5,5-dimethyl-1-pyrroline N-oxide (DMPO) was purchased from Dojindo Co. Ltd. Poly(vinylpyrrolidone) (PVP) was used for the preparation of iodophor disinfectant.

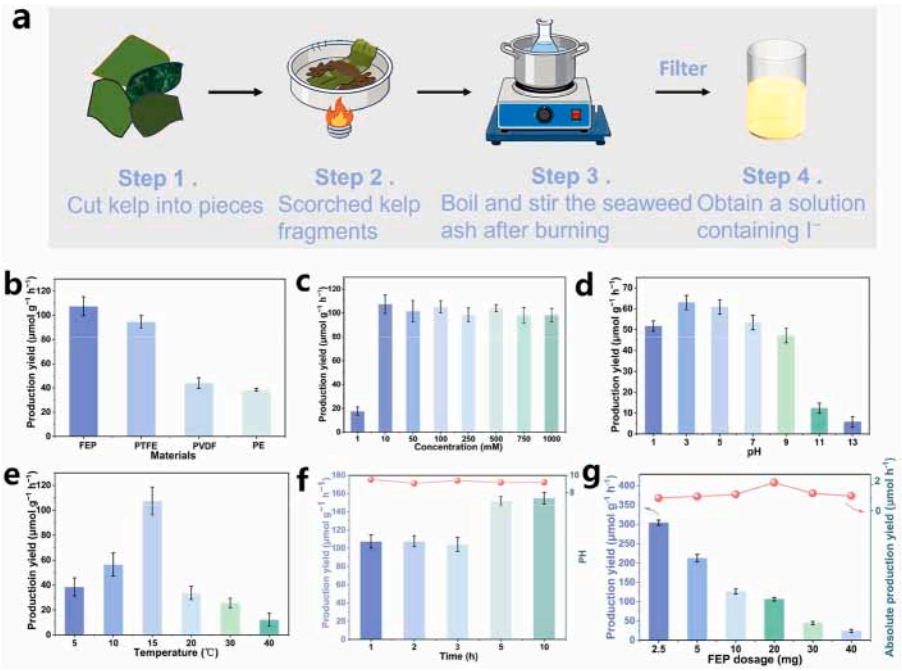


Fig. 2. Mechanistic study and parameter optimization for iodide extraction from kelp: a) Schematic diagram of the process for extracting I^- from kelp. b) Comparison of production yields for different materials (FEP, PTFE, PVDF, PE). c) Investigation of the relationship between concentration changes and production yield. d) Demonstration of the effect of pH on production yield. e) Study of differences in production yield under varying temperatures. f) Observation of the relationship between reaction time and production yield. g) Analysis of the effect of FEP amount on production yield.

2.3. Sample preparation

2.3.1. Preparation of KI solution and reaction system

Taking the optimal experimental conditions as an example, 0.166 g of solid KI was placed in a beaker, and about 50–70 mL of deionized water was added and stirred until completely dissolved. The solution was then transferred to a 100 mL volumetric flask and diluted to volume to obtain 100 mL of a 10 mM KI solution. Then, 20 mg of FEP powder was weighed and added to a bottle containing 10 mL of the prepared KI solution, followed by a 1-h ultrasonic bath at a constant temperature (KQ500GDV, 40 kHz, 500 W) to facilitate CE-Chemistry with the temperature maintained at 15 °C. Anaerobic or aerobic conditions were achieved by introducing argon (Ar) or oxygen (O_2), respectively. Before ultrasonic treatment, Ar or O_2 was introduced for 15 min to purge the air from the reaction system, and continuous introduction of the gas was maintained during ultrasonic treatment until the end of the reaction.

2.3.2. Plotting the I_3^- standard curve

I_3^- standard solutions were synthesized by adding a large excess of I^- to aqueous solutions of I_2 with known concentrations to form I_3^-. The concentration of I_3^- was quantitatively measured by the absorbance at 352 nm, and a corresponding standard curve was plotted. To ensure that aqueous I_2 was completely converted to I_3^-, solutions were prepared with different I^-:I_2 molar ratios ranging from 20:1 to 2000:1, with the concentration of aqueous I_2 fixed at 0.05 mM. As the I^-:I_2 ratio gradually increased, the absorbance initially increased rapidly, then reached a saturation value and remained at a relatively high level (eventually close to 1.6). The absorbance at 352 nm (the characteristic peak of I_3^-) became stable when the I^-:I_2 ratio was higher than 500:1, indicating that aqueous I_2 was almost completely converted to I_3^-. Therefore, a 1000:1 molar ratio was chosen as the optimal ratio for preparing the I_3^- standard solution dilution series.

2.3.3. Calculation of I_3^- production yield

The formula for calculating the production yield S (μmol g^{-1} h^{-1}) of I_3^- after the reaction is:

$$s = \frac{C \times V}{m\ t} \times 100\%$$

Where C is the measured concentration of I_3^- generated from I^- oxidation, V is the volume of KI solution added, m is the mass of dielectric powder added, and t is the reaction time.

2.3.4. Preparation and treatment of kelp extract

Dried kelp was crushed and combusted to convert iodides into water-soluble inorganic iodine salts. Deionized water was added, and the mixture was extracted at 100 °C for 1 h under magnetic stirring to enhance mass transfer and ensure the complete dissolution of I^- in the aqueous solution. The successful release of iodine-containing substances was verified by adding H_2O_2 to oxidize I^- to I_2, followed by starch reagent, which induced an immediate blue-purple color change. The obtained I^--rich aqueous solution was then subjected to ultrasonic treatment, where ultrasound-assisted CE-Chemistry drove the directional oxidation of I^- to I_3^- via hydroxyl radicals generated in situ at the dielectric L-S interface. Finally, the resulting iodine-containing product was complexed with PVP to form an iodophor disinfectant. The flowchart for iodide ion extraction is illustrated in Fig. 2a.

Quantitative analysis of iodide ions was performed using a Shimadzu HIC-20A SUPER ion chromatograph equipped with an anion suppressor, a conductivity detector, and a UV detector, with a mobile phase of 3.5 mM sodium carbonate-10 mM sodium bicarbonate, eluted isocratically at a flow rate of 1.2 mL/min, and an injection volume of 400 μL. The iodide ion concentrations in extracts obtained with 50, 80, and 100 mL solvent were 445.66, 253.45, and 200.82 mg/L, respectively, showing a decreasing trend with increasing solvent volume. The average iodide concentration was calculated as 299.98 mg/L, with a concentration range of 200.82–445.66 mg/L. All measured iodide concentrations exceeded 200 mg/L and were within the concentration range of reagent-grade KI used, confirming that the detection sensitivity meets the requirements of subsequent experiments. Additionally, fluoride ions were quantitatively analyzed to check for potential fluoride leakage, and no fluoride ions were detected in the reaction system.

2.3.5. Construction of synthetic iodide system

This study selected KI, NaI, and LiI as experimental salt solutions to simulate the ionic environment of actual kelp extract and to investigate the regulatory effects of ionic composition and concentration on the CE-Chemistry. Ion chromatography (IC) and inductively coupled plasma (ICP) analysis showed that the average concentration of iodide ions in kelp extract was 299.98 mg/L. The extract also contained cations such as Na^+, K^+, Ca^{2+}, and Mg^{2+}, as well as anions such as carbonate and bicarbonate. Based on these compositional characteristics, the above salt solutions were used to construct a synthetic iodide system, providing a controllable experimental model for subsequent reaction parameter optimization and laying a research foundation for applying this method to actual kelp extract. This study used kelp, a marine biomass that is abundant, low-cost, and carbon-neutral, as a natural iodine source. After efficiently extracting iodide ions through green methods such as pyrolysis and boiling, the CE-Chemistry method assisted by ultrasound and without adding oxidizing agents achieved efficient oxidation of I^- from kelp extract to I_3^-.

2.4. Sample characterizationand quantitativeanalysis

2.4.1. Material characterization methods

UV–Vis spectra: Recorded in the range of 200–700 nm using a Hitachi UV-4150 UV–Vis spectrometer. SEM images: Obtained using FEI Nova 450. Energy dispersive X-ray (EDX): Performed on an FEI Nova 450 equipped with an AMETEK Octane Super appendix; EDX spectra were also obtained on the FEI Tecnai F20. FTIR spectra: Recorded in the range of 400 to 2000 cm^{-1} on a Bruker Vertex 80 V. Raman spectra: Recorded on LabRam HR evolution (HORIBA, SAS France) using a range of 200 to 2000 cm^{-1}. NAP-XPS: The chemical state of FEP before and after the reaction was characterized by near-atmospheric X-ray photoelectron spectrometry (NAP-XPS, SPECS, Germany). XRD: X-ray diffraction (XRD) of FEP was measured using an Advance diffractometer (Bruker-D8, Germany) at an operating voltage of 40 kV. HPLC-MS analysis: Performed using the Thermo Scientific Q Exactive Orbitrap Quadrupole-Electrostatic Field Orbitrap High-Resolution Tandem Mass Spectrometer; the HESI ion source of the mass spectrometer was set to 3.5 kV and operated in positive/negative ion mode, the mass spectrometry scanner was set to a full scan range of 100–1000 *m/z*, and the instrument had a resolution of 70,000 FWHM. HRTEM images: Obtained on the FEI Tecnai F20. EPR: Electron paramagnetic resonance (EPR) was recorded on the Bruker EMX Plus 9.5/12/P/L; the measurement was performed in the X-band (9.830243 GHz) with an amplitude modulation of 1 G, a microwave power of 2 mW, an amplitude modulation frequency of 100 kHz, a conversion time of 60.00 ms, and a time constant of 40.96 ms.

2.4.2. Quantitative analysis of ions in kelp extract

Fluoride ion detection: Quantitative analysis of fluoride ions was conducted to evaluate potential fluoride ion leaching from FEP during the reaction, and no detectable fluoride ions were found in the reaction system, confirming the chemical stability of FEP.

2.5. DFT methods

First-principles calculations were carried out within DFT using the projector-augmented wave (PAW) method, as implemented in the Vienna Ab-initio Simulation Package (VASP) [40–43]. The exchange-correlation energy was described using the Perdew-Burke-Ernzerhof (PBE) functional within the generalized gradient approximation (GGA) [44]. A plane-wave cutoff energy of 550 eV was employed. Structural optimizations were performed until the Hellmann-Feynman forces on each atom were <0.01 eV/Å, and the total energy change between successive self-consistent steps was below 1×10^{-5} eV.

3. Result and discussion

3.1. Iodide activation through CE-Chemistry

The effects of salt solution type and dielectric material on the ultrasound-assisted CE-Chemistry synthesis of I_3^- were first evaluated to establish optimal reaction conditions. Among the tested electrolytes, the ionic composition strongly influenced the production yield of I^- oxidation, highlighting the critical role of the interfacial ionic environment in modulating charge transfer [45,46]. Similarly, dielectric materials with distinct surface properties yielded markedly different I_3^- production, indicating that both surface chemistry and triboelectric characteristics govern radical generation and directional electron transfer efficiency. To further elucidate factors controlling reaction efficiency, key parameters, including pH, temperature, reaction time, I^- concentration, ambient atmosphere, and dielectric dosage, were systematically investigated. Concentrations of I_3^- were determined from absorbance at 352 nm using a standard curve (Fig. S1-S3), prepared by adding excess KI to aqueous I_2 solutions until saturation. The results indicate that alkaline conditions and elevated temperatures accelerate I^- oxidation, whereas extended reaction times gradually increase production yield but eventually plateau, suggesting a balance between radical availability and EDL-mediated screening effects. Increasing I^- concentration and dielectric dosage proportionally enhanced I_3^- formation, consistent with the role of interfacial charge density in driving CE-Chemistry, while variations in ambient atmosphere confirmed that oxygen plays only a secondary role, with in situ generated •OH radicals serving as the primary oxidants. As shown in Fig. 2b, the choice of dielectric material strongly influences I_3^- production yield: FEP, PTFE, PVDF and PE. The properties of FEP are shown as Table S1. In addition, the I_3^- yields and the order in the triboelectric series under the same experimental conditions are shown in Table S2. The influence of catalyst particle size on I_3^- production yield was systematically investigated. As illustrated in Fig. S4, a pronounced difference in catalytic performance was observed between nanoscale and microscale FEP powder. Specifically, the nanoscale catalyst provides a significantly higher yield, while its microscale counterpart accounts for only one-third under the same experimental conditions. This size-dependent activity can be attributed to the larger specific surface area and more abundant reactive sites provided by the nanoscale particles, which facilitate enhanced interfacial charge transfer and subsequent radical generation during the ultrasound-assisted CE-Chemistry. Fig. S5 shows that the I_3^- yield increased significantly with increasing iodide concentration in the low-concentration range (1–10 mM). As shown in Fig. 2c, when the concentration exceeded 10 mM, the yield gradually plateaued and no longer increased obviously. These results confirm the existence of an interfacial iodide supply insufficiency effect, and concentration ceases to be the dominant factor above 10 mM. Fig. 2d shows that the I_3^- yield gradually increased as the solution pH decreased from 13 to 3, and the highest yield was achieved under acidic conditions. On one hand, acidic conditions can extend the lifetime of electrons, reduce the recombination of electrons with iodine atoms, and drive the oxidation equilibrium of I^- forward; on the other hand, supplying sufficient protons for the reaction can significantly enhance the production yield of I_3^- and I_2, providing the necessary conditions for the reaction [38–40]. Temperature dependence (Fig. 2e) exhibits an initial increase followed by a decline, peaking at ~15 °C, which correlates with the glass transition temperature of FEP (~35 °C) and its declining electron extraction efficiency at higher temperatures. The glass transition temperature of FEP and the temperature-dependent behavior of interfacial charge transfer and electron extraction efficiency in CE-Chemistry have been well documented in previous studies [47–49]. Reaction time studies (Fig. 2f) show gradual production yield increases, stabilizing after 1 h, with solution pH remaining constant. As shown in Fig. 2g, the reaction production yield exhibits a clear dependence on the dosage of the FEP [29,50]. With increasing FEP amount, the production yield of I_3^- initially rises and reaches a maximum at 20

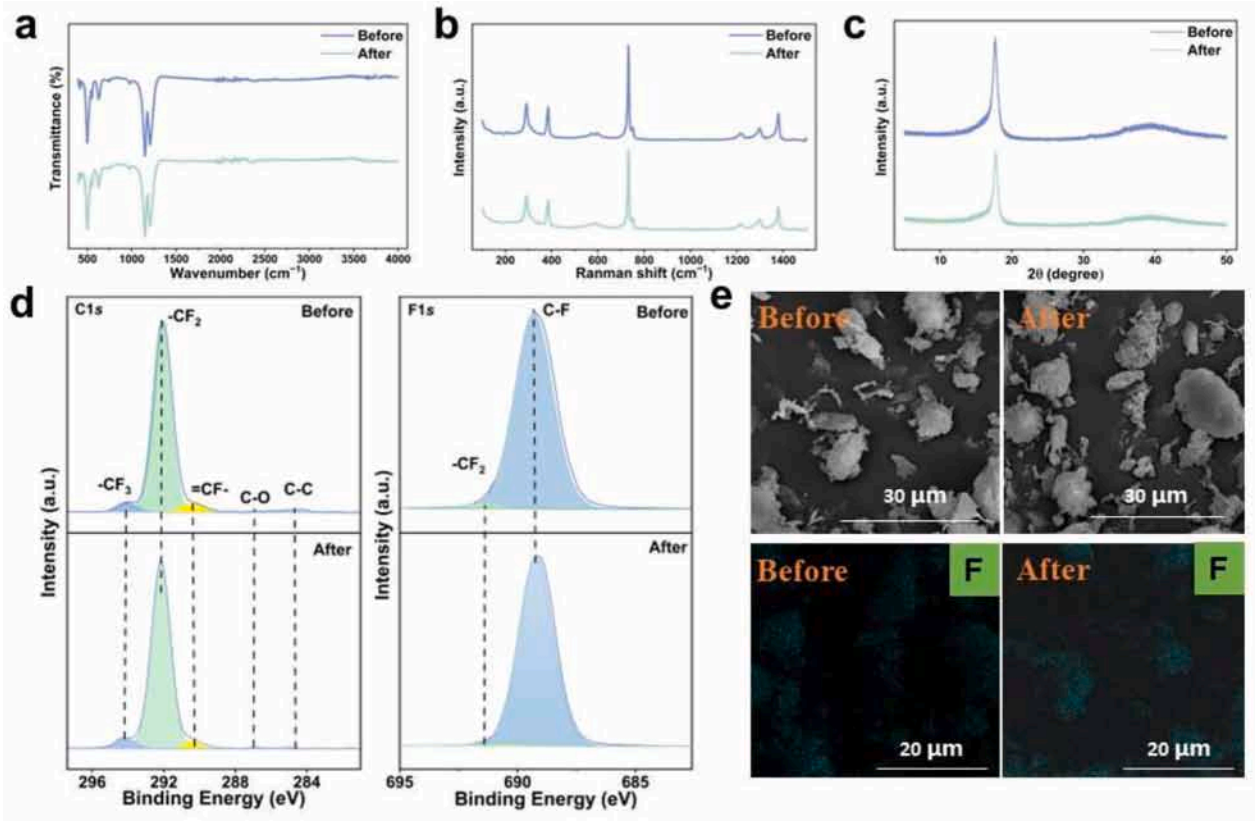


Fig. 3. Characterization of FEP before and after CE-Chemistry: a-c) FTIR spectra, Raman spectra, and XRD spectra of FEP before and after the CE-Chemistry. d) C1*s* and F1*s* XPS spectra of FEP powder before and after the CE-Chemistry reaction. e) Morphological characterization and EDX analysis of FEP before and after the reaction.

mg of FEP, indicating that this loading provides the most favorable conditions for intrinsic reaction kinetics under the present experimental configuration. At higher dosages, however, the production yield declines, likely due to the scattering of ultrasonic waves by excess dielectric powder and reduced effective interfacial area per unit mass. Notably, when reaction performance is evaluated on a mass-normalized basis, a different trend emerges. A lower FEP loading of 2.5 mg generates a markedly higher I_3^- production yield per gram of FEP than the 20 mg case, indicating more efficient utilization of active material at low loadings. This result reveals an inherent trade-off between maximizing the absolute production yield and optimizing mass-specific reaction efficiency [50]. While reduced FEP dosages favor cost-effective operation and economy, intermediate loadings provide higher overall production yields and are therefore more suitable for mechanistic and kinetic studies. Integrating these considerations with the systematic parameter optimization shown in Fig. 2, the optimal conditions for I_3^- synthesis are identified as 15 °C, 10 mL of 10 mM KI solution, and 20 mg FEP, under which the reaction reaches a maximum I_3^- concentration of 214.89 μM and a production yield of 107.45 μmol g^{-1} h^{-1}.

4. Recyclability and stability of the dielectrics

The stability and recyclability of FEP as a dielectric material were systematically evaluated to assess its suitability for sustainable CE-Chemistry. After the reaction, the recovered powder was washed with deionized water and characterized using multiple spectroscopic and microscopic techniques. Raman spectra confirmed that the backbone vibration modes remained unchanged (Fig. 3a), and Fourier transform infrared (FTIR) spectra showed a stable fingerprint region below 1500 cm^{-1} (Fig. 3b). X-ray diffraction (XRD) analysis indicated no shift in diffraction peaks, confirming preservation of the crystal structure (Fig. 3c), while X-ray photoelectron spectroscopy (XPS) measurements revealed no changes in binding energies or the appearance of new peaks, demonstrating chemical state stability (Fig. 3d). Scanning electron microscopy (SEM) imaging and the spectrum of the F element in the energy-dispersive X-ray spectroscopy (EDX) elemental distribution map further confirmed the retention of morphology and composition, with almost no change in particle size and no signs of decomposition (Fig. 3e). Importantly, the reaction performance of FEP remained essentially unchanged over 50 reaction cycles (Fig. S6), demonstrating excellent recyclability. In addition, the analysis of total organic carbon (TOC) in the reaction system showed that the changes in organic carbon concentration were negligible (Fig. S7), further indicating the absence of carbon leaching or structural decomposition during the CE chemical process [34]. And as shown in Fig. S8, the change in zeta potential of FEP in water before and after the reaction is not significant, indicating that the surface chemical structure and charged state of FEP remain basically unchanged during the catalytic process, demonstrating excellent structural and interfacial stability [36]. Furthermore, previous studies have confirmed that fluoropolymers such as FEP can maintain atomic-level surface smoothness with no significant change in surface roughness after long-term cycles in ultrasound-driven CE-Chemistry systems, further verifying their excellent mechanical robustness [51,52]. Collectively, these results establish that FEP is chemically inert, mechanically robust, and fully reusable, enabling cost-effective, sustainable CE-Chemistry without reliance on precious-metal catalysts.

5. Reaction mechanism

The mechanism of iodide activation via CE-Chemistry was next examined. As illustrated in Fig. 4a, water molecules at the dielectric L-S interface are first activated to generate •OH radicals, which oxidize I^- to

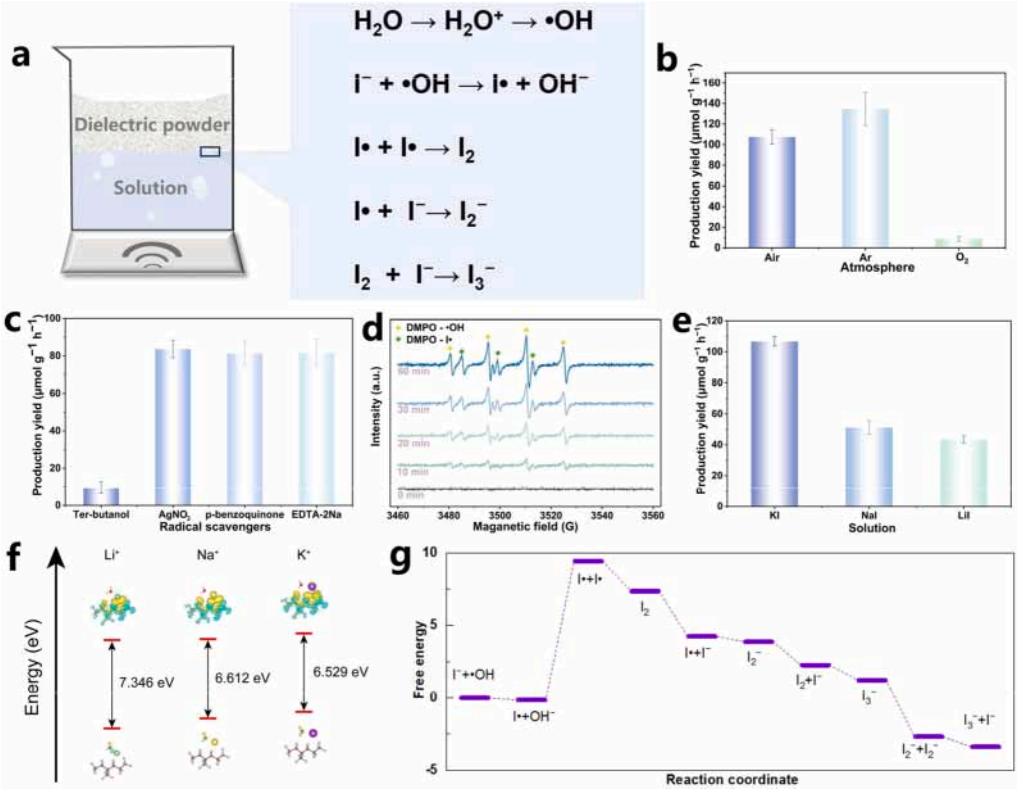


Fig. 4. Experimental principles and free radical verification: a) Schematic diagram of the experimental setup and explanation of the experimental principle. b) Effects of aerobic and anaerobic conditions on I_3^- yield. c) The effects of different radical scavengers on I_3^- yield, including tert-butanol, $AgNO_3$, p-benzoquinone, and EDTA-2Na, which are respectively considered scavengers of hydroxyl radicals, superoxide radicals, hole and electrons. d) ESR spectra of the DMPO-trapped radical adducts. e) Effect of different salt solutions on the yield of I_3^-. f) DFT simulations of electron transfer energy barriers in different ions. g) Free energy profile for the oxidation of I^- to form I_3^-.

I•. The resulting I• then reacts with I^- in solution to form I_2 (*m/z*254), which subsequently combines with an additional I^- to yield I_3^- (*m/z*381, Fig. S9). Environmental atmosphere experiments further revealed that I_3^- yields are significantly higher under an Ar atmosphere compared with air or O_2 (Fig. 4b), indicating that removal of O_2 minimizes competition for interfacial electrons and maximizes •OH generation for efficient I^- oxidation [53,10]. The role of reactive species was probed using scavengers: addition of $AgNO_3$, EDTA-2Na, or p-benzoquinone had negligible effect on I_3^- formation, whereas tert-butanol, a •OH scavenger, markedly suppressed oxidation efficiency (Fig. 4c), confirming the central role of •OH in I^- activation. Electron spin resonance (ESR) spectroscopy using DMPO (5,5-dimethyl-1-pyrroline N-oxide) as a spin trap directly verified the generation of •OH and I• under CE-Chemistry conditions, producing characteristic 1:2:2:1 signal of DMPO-•OH, along with a clear 1:1:1 triplet signal corresponding to DMPO-I• (Fig. 4d) [1]. In contrast, samples without CE-Chemistry treatment showed no detectable ESR signals within the same time frame (Fig. S9), demonstrating that •OH and I• formation is uniquely facilitated by interfacial charge transfer under CE-Chemistry.

Additional experiments were performed using different salt solutions to investigate the influence of cation species on the EDL structure and interfacial triboelectric field. By modulating cation hydration size, the local EDL and triboelectric field at the L-S interface could be effectively tuned, directly impacting reaction kinetics. As shown in Fig. 4e, the I_3^- yield follows the order $K^+ > Na^+ > Li^+$, which is inversely correlated with the cation hydration radii ($K^+ < Na^+ < Li^+$, summarized in Supplementary Material Table S4). This trend aligns perfectly with the calculated electron transfer energy barriers at the FEP/solution interface, where a smaller hydration radius corresponds to a lower barrier, confirming the critical role of cation hydration in regulating interfacial charge transfer and iodide oxidation performance. To further elucidate the underlying regulatory mechanism, systematic DFT calculations were performed, with results depicted in Fig. 4f and g As shown in Fig. 4f, the introduction of Li^+, Na^+ and K^+ significantly elevates the interfacial electron transfer barrier, following the order $Li^+ > Na^+ > K^+$, which is fully consistent with the sequence of cation hydration radii. This indicates that K^+, with its smaller hydration radius, weakly perturbs the EDL at the FEP interface, thereby reducing the electron transfer barrier and facilitating the participation of CE-Chemistry-generated free electrons in iodide oxidation, which thermodynamically explains the significantly higher I_3^- yield observed experimentally in the K^+ system. Meanwhile, Fig. 4g illustrates the Gibbs free energy pathway for iodide oxidation to I_3^-: the reaction initiates with the oxidation of I^- by •OH, and the free energy decreases overall along the entire reaction pathway, this is completely consistent with the reaction mechanism in Fig. 4a, confirming the thermodynamic feasibility of efficient •OH-driven iodide oxidation to I_3^- at the FEP interface. Collectively, these theoretical results are in excellent agreement with the experimentally observed cation effects, systematically uncovering the core role of cations in regulating FEP L-S interfacial charge transfer and the iodide oxidation pathway, and providing a solid theoretical foundation for understanding cation regulation in CE-Chemistry systems [54]. Smaller hydrated cations promote the formation of a denser Stern layer, generating a stronger interfacial electric field. This denser, negatively charged EDL enhances anion accumulation by strengthening local charge shielding and reducing repulsion in the diffusion layer. Therefore, under the same conditions, the EDL in KCl solution is more compact than in NaCl or LiCl solutions. Consequently, smaller cation hydration radii increase the local concentration of I^- in the reaction zone, significantly improving the efficiency of iodine conversion. These results provide direct experimental evidence that the interfacial field, influenced by EDL structure, is a key factor controlling CE-Chemistry reaction kinetics.

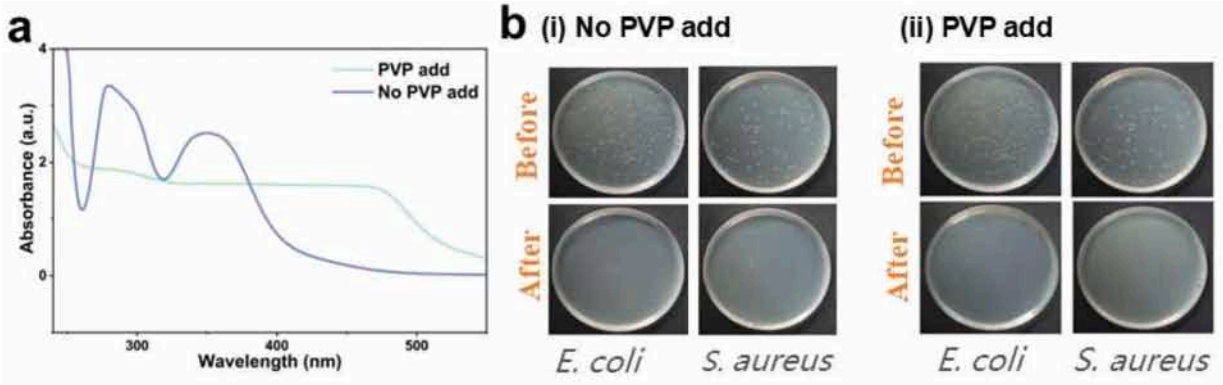


Fig. 5. Preparation of PVP-I and its antibacterial performance testing. a) Comparison of the UV spectra before and after adding PVP to the I_3^- solution. b) Images of the plates showing colony formation after disinfection, before (i) and after (ii) adding PVP.

6. Preparation of iodine-based disinfectants from kelp

Kelp, a marine biomass rich in iodine, predominantly contains iodine as I^-. Environmentally friendly extraction of I^- is a prerequisite for its subsequent transformation into active iodine species and preparation of iodophor disinfectants via CE-Chemistry. Following extraction, complexation of the high-concentration I_3^- solution with an appropriate amount of PVP yielded a brownish-yellow povidone-iodine (PVP-I) reagent (Fig. S10). UV–visible spectroscopy (Fig. 5a) shows that, upon addition of PVP, the characteristic absorption peaks at 288 nm and 352 nm decreased substantially or disappeared, while a new peak emerged at ~470 nm, confirming formation of the PVP-I complex. The antibacterial performance of the resulting PVP-I solution was evaluated alongside the uncomplexed I_3^- solution. Both demonstrated potent disinfection activity, achieving up to 99.9999% reduction of *E.coli*and *Staphylococcus aureus* (Fig. 5b), highlighting the high efficacy of the CE-Chemistry, generated iodine species for antimicrobial applications.

7. Conclusion

In this study, kelp was employed as a natural iodine source, and an oxidant-free, ultrasound-assisted CE-Chemistry strategy is proposed toward potentially achieving efficient iodine extraction and conversion under ambient conditions, with high tolerance to pH and ionic variations. Iodide released through pyrolysis and boiling was directionally oxidized via in situ •OH generation via CE-Chemistry, producing I_3^- at 107.45 μmol g^{-1} h^{-1}. Subsequent complexation with poly(vinylpyrrolidone) affords a high-performance iodophor disinfectant, achieving a 6-log (99.9999%) reduction of *Staphylococcus aureus* and *E. coli*. Mechanistic studies reveal that the dynamic regulation of the EDL at the dielectric solid-liquid interface governs CE-Chemistry kinetics. By varying cation hydration size ($K^+ < Na^+ < Li^+$), the local Stern layer density and interfacial electric field are tuned, modulating I^- anion accumulation and directly enhancing reaction efficiency. This provides direct experimental evidence linking EDL structure to reaction kinetics, highlighting the pivotal role of interfacial electric field in CE-Chemistry. Overall, this work extends CE-Chemistry to marine biomass valorization for the first time, offering a sustainable, low-cost route to high-value iodophors. It establishes a general framework for EDL-mediated interfacial reaction, provides mechanistic insight into reaction dynamics, and lays the foundation for environmentally friendly, scalable iodine-based disinfection strategies.

CRediT authorship contribution statement

Xinyi Huo: Writing – original draft, Investigation. **Han Qian:** Writing – original draft, Visualization, Methodology, Investigation, Data curation. **Ning Wu:** Data curation, Investigation, Methodology. **Zeyang Yu:** Data curation, Formal analysis. **Bing Sun:** Writing – review & editing, Investigation. **Zhong Lin Wang:** Writing – review & editing, Investigation, Funding acquisition. **Di Wei:** Writing – review & editing, Supervision, Investigation, Funding acquisition.

Declaration of competing interest

The authors declare that they have no known competing financial interests or personal relationships that could have appeared to influence the work reported in this paper.

Acknowledgments

The authors sincerely thank the support of the National Natural Science Foundation of China (Project No 22479016) for this research.

Supplementary materials

Supplementary material associated with this article can be found, in the online version, at doi:10.1016/j.electacta.2026.148894.

Data availability

Data will be made available on request.

References

[1] A. Fernando, S. Parajuli, K.K. Barakoti, W. Miao, M.A. Alpuche Aviles, Evidence of radical intermediate generated in the electrochemical oxidation of iodide, J. Mex. Chem. Soc. 63 (2019).
[2] L. Li, J. Wu, A. Xia, X. Zhu, Q. Liao, Tandem mechano-enzymatic Catalysis: a green revolution in lignocellulosic biomass pretreatment via contact-electro-catalysis, ACS Sustain. Chem. Eng. 13 (2025) 8508–8514.
[3] D. Xing, X. Yuan, C. Liang, T. Jin, S. Zhang, X. Zhang, Spontaneous oxidation of I^- in water microdroplets and its atmospheric implications, Chem. Commun. 58 (2022) 12447–12450.
[4] T.W. Xingming Tao, L. Tan, F. Xu, A. Chen, Y. Yang, R. Zhang, X. Wang, High-performance constant current triboelectric nanogenerator for wind energy harvesting and air purification, SmartSys 1 (2025).
[5] T. Jia, W. Wang, C. Zhang, L. Zhang, W. Wang, Polydopamine-mediated contact-electro-catalysis for efficient partial oxidation of methane, Angew. Chem. Int. Ed. 64 (2025) e202413343.
[6] W.L. Rongyao Wang, S. Wang, B. Du, X. Bai, H. Yan, D. Gao, W.G. Xiaohua Ren, F. R. Fan, G.Z. Chen, Directional electron transfer in island-sea structured contact-electro-catalysis enables cascade defluorination of PFAS, Angew. Chem. Int. Ed. (2025) e25861.
[7] Z. Xu, J. Yang, P. Sun, Y. Chen, Z. Ji, X. Wang, M. Xu, J. Li, L. Pan, Iodide-mediated intermediate regulation strategy enables high-capacity and ultra-stable zinc–iodine batteries, Chem. Sci. 16 (2025) 13211–13220.
[8] X. Huo, S. Li, B. Sun, Z.L. Wang, D. Wei, Recent progress of chemical reactions induced by contact electrification, Molecules 30 (2025) 584.
[9] Q. Li, D.D. Ma, J. Zhao, W. Wei, S.G. Han, X.T. Wu, R. Zou, Q. Xu, Q.L. Zhu, Modular synchronous synthesis of amides and α-ketoamides realized by matching electrolysis-paired tandems, Angew. Chem. Int. Ed. 64 (2025) e202503440.

[10] J. Zhao, X. Zhang, J. Xu, W. Tang, Z. Lin Wang, F. Ru Fan, Contact-electro-catalysis for direct synthesis of H_2O_2 under ambient conditions, Angew. Chem. Int. Ed. 62 (2023) e202300604.

[11] Z. Chen, Y. Zhang, P. Lv, T. Wu, J. He, J. Du, Q. Sun, Q. Wu, J. Yang, Y. Zhang, Y. Zhang, F. He, C. Cui, G. Hong, H. Zhu, Y. Li, J. Guo, X. Deng, Hand-powered interfacial electric-field-enhanced water disinfection system, Nat. Nanotechnol. (2025).

[12] H.H. Dhanjee, A. Saebi, I. Buslov, A.R. Loftis, S.L. Buchwald, B.L. Pentelute, Protein–Protein cross-coupling via palladium–Protein oxidative addition complexes from cysteine residues, J. Am. Chem. Soc. 142 (2020) 9124–9129.

[13] H.A. Fernandez, L.K. Weavers, The impact of inorganic salts on the ultrasonic degradation of contaminants: a review, Ultrason. Sonochem. 111 (2024) 107076.

[14] C. Gu, Q. Yang, X. Zhang, R. Feng, S. Wang, T. Liu, P. He, H. Yin, J. Zhu, M. Gan, Bioengineered iron-based heterojunction orientation in optimizing activation pathways for superoxide radical-mediated photoreduction of Cr(VI) from water, Water Res. 283 (2025) 123832.

[15] Y.X. Bolei Chen, R.X. He, H.Q. Sang, W.C. Zhang, J. Li, L.F. Chen, P. Wang, S. S. Guo, Y.G. Yin, L. Hu, M.Y. Song, Y. Liang, Y.W. Wang, G.B. Jiang, RN. Zare, Water–solid contact electrification causes hydrogen peroxide production from hydroxyl radical recombination in sprayed microdroplets, Proc. Natl. Acad. Sci. 119 (2022) e2209056119.

[16] H. Li, A. Xie, C. Hong, Z. Wang, X. Chu, Z.L. Wang, Y. Liu, P. Jiang, Hydroxyl radical generation from H_2O_2 *via* liquid–liquid contact-electro-catalysis, Chem. Sci. 16 (2025) 20580–20593.

[17] S. Li, Z. Zhang, P. Peng, X. Li, Z.L. Wang, D. Wei, A green approach to induce and steer chemical reactions using inert solid dielectrics, Nano Energy 122 (2024) 109286.

[18] F.G. Thiago, A.L. Burgo, G.H. Pollack, Where is water in the triboelectric series, J. Electrostat. 80 (2016) 30–33.

[19] Z. Wang, X. Dong, X.-F. Li, Y. Feng, S. Li, W. Tang, Z.L. Wang, A contact-electro-catalysis process for producing reactive oxygen species by ball milling of triboelectric materials, Nat. Commun. 15 (2024) 757.

[20] C. Xu, Y. Zi, A.C. Wang, H. Zou, Y. Dai, X. He, P. Wang, Y.C. Wang, P. Feng, D. Li, Z. L. Wang, On the electron-transfer mechanism in the contact-electrification effect, Adv. Mater. 30 (2018) 1706790.

[21] Y. Zhao, Y. Liu, Y. Wang, S. Li, Y. Liu, Z.L. Wang, P. Jiang, The process of free radical generation in contact electrification at solid-liquid interface, Nano Energy 112 (2023) 108464.

[22] A.R.L. El-Kazzaz, A.C. Rose-Innes, Contact charging of insulators by liquid metals, J. Electrost 16 (1985) 157–163.

[23] K.H. Yatsuzuka, Y, K. Asano, Electrification of polymer surface caused by sliding ultrapure water, J. Electrost. 3 (1994) 157–171.

[24] S. Lin, L. Xu, A. Chi Wang, Z.L. Wang, Quantifying electron-transfer in liquid-solid contact electrification and the formation of electric double-layer, Nat. Commun. 11 (2020) 399.

[25] S. Lin, X. Chen, Z.L. Wang, Contact electrification at the liquid–Solid interface, Chem. Rev. 122 (2022) 5209–5232.

[26] T.L.D Wei, C. Kvarnstrom, L. Kronberg, R. Sjoholm, A. Ivaska, Electrosynthesis and characterisation of poly (N-methylaniline) in organic solvents, J. Electroanal. Chem. 575 (1) (2025) 19–26.

[27] T.C. Xiang Li, Z.L. Wang, D. Wei, Neuromimetic circuits enabled by dynamic regulation of the electrical double layer, Npj Flex Electron 9 (2025).

[28] Z.L.W. Xiang Li, D. Wei, Iontronic logic control driven by dynamic electrical double layer regulation, Iontronics 1 (2025).

[29] X.F.L. Berbille Andy, Y. Su, S. Li, X. Zhao, L. Zhu, Z.L. Wang, Mechanism for generating H_2O_2 at water-solid interface by contact-electrification, Adv. Mater. 35 (2023) 2304387.

[30] Z. Yu, X. Li, W. Ning, S. Yue, C. Xiang, Z. Yue, Q. Siyao, W. Xucong, G. Hao, M. Zifei, W. Morten, L. Ning, W.Z. Lin, B. Zhenfeng, C. Xiangyu, Largely enhanced photocatalysis process by contact-electro-catalysis for efficient and eco-friendly recovery of gold, Adv. Mater. (2025) e14244.

[31] N. Wang, W. Jiang, J. Yang, H. Feng, Y. Zheng, S. Wang, B. Li, J.Z.X. Heng, W. C. Ong, H.R. Tan, Y.W. Zhang, D. Wang, E. Ye, Z. Li, Contact-electro-catalytic CO2 reduction from ambient air, Nat. Commun. 15 (2024) 5913.

[32] Z. Wang, A. Berbille, Y. Feng, S. Li, L. Zhu, W. Tang, Z.L. Wang, Contact-electro-catalysis for the degradation of organic pollutants using pristine dielectric powders, Nat. Commun. 13 (2022) 130.

[33] T. Gan, Z. Yang, S. Li, H. Qian, Z. Li, J. Liu, P. Peng, J. Bai, H. Liu, Z. Wang, D. Wei, Unveiling Janus chemical processes in contact-electro-chemistry through oxygen reduction reactions, J. Am. Chem. Soc. 147 (2025) 25407–25416.

[34] T. Gan, Z. Li, S. Li, H. Liu, G. Amaratunga, Z. Wang, D. Wei, Sustainable fluorinated silicon dielectric design for enhanced contact-electro-chemistry, Angew. Chem. Int. Ed. 64 (2025) e202517059.

[35] T.Y. Lui, X. Chen, S. Zhang, D. Hu, T.-W. Dominic Chan, Peptide oxidation induced by liquid–Solid contact electrification as revealed in liquid microjunction-surface sampling probe mass spectrometry, Anal. Chem. 95 (2023) 9060–9067.

[36] J. Liu, Z. Yang, S. Li, Y. Du, Z. Zhang, J. Shao, M. Willatzen, Z.L. Wang, D. Wei, Nonaqueous contact-electro-chemistry via triboelectric charge, J. Am. Chem. Soc. 146 (2024) 31574–31584.

[37] C. Xu, S. Li, Z. Yang, M. Willatzen, Z. Lin Wang, D. Wei, Contact-electro-luminescence triggered by triboelectric charge, Chem. Eng. J. 501 (2024).

[38] J.L. Zhang, S, Z.L Wang, Electrostatic charges regulate chemiluminescence by electron transfer at the liquid–Solid interface, J. Phys. Chem. B 126 (2022) 2754–2760.

[39] X. Zhao, Y. Su, A. Berbille, Z.L. Wang, W. Tang, Degradation of methyl orange by dielectric films based on contact-electro-catalysis, Nanoscale 15 (2023) 6243–6251.

[40] K.W. Hohenberg P, Inhomogeneous electron gas, Phys. Rev. B: Condens. Matter 136 (1964) B864–B871.

[41] S.L. Kohn W, Self-consistent equations including exchange and correlation effects, Phys. Rev. 140 (1965) A1133–A1138.

[42] J.D. Kresse G, From ultrasoft pseudopotentials to the projector augmented-wave method, Phys. Rev. B: Condens. Matter 59 (1999) 1758–1775.

[43] P.E.. Blöchl, Projector augmented-wave method, Phys. Rev. B 50 (1994) 17953–17979.

[44] K.B.A.M.E.J.P. Perdew. Physical review letters 77 (1996) 3865.

[45] Z.W. Puguang Peng, D. Wei, Modulating multi-ion dynamics for high-performance iontronic systems, Iontronics 2 (2026).

[46] D. Wei, IONTRONICS inaugural editorial: defining a new frontier with iontronics, Iontronics 1 (2025) 1.

[47] A.C.W. Cheng Xu, H. Zou, B. Zhang, C. Zhang, Y. Zi, L. Pan, P. Wang, P. Feng, Z. Lin, Z.L. Wang, Raising the working temperature of a triboelectric nanogenerator by quenching down electron thermionic emission in contact-electrification, Advancved Materials 30 (2018) 1803968.

[48] Y.Z. Haiyang Zou, L. Guo, P. Wang, X. He, G. Dai, H. Zheng, C. Chen, A.C. Wang, C. Xu, Z.L. Wang, Quantifying the triboelectric series, Nat. Commun. 10 (2019) 1427.

[49] X.H.Y. Sun, S. Soh, Solid-to-liquid charge transfer for generating droplets with tunable charge, Angew. Chem. Int. Ed. 55 (2016) 9956.

[50] W. Li, J. Sun, M. Wang, J. Xu, Y. Wang, L. Yang, R. Yan, H. He, S. Wang, W. Q. Deng, Z.Q. Tian, F.R. Fan, Contact-electro-catalysis for direct oxidation of methane under ambient conditions, Angew. Chem. Int. Ed. 63 (2024) e202403114.

[51] Z.Z.S Li, F. Yang, X. Li, P. Peng, Y. Du, Q. Zeng, M. Willatzen, Z.L. Wang, D. Wei, Transistor-like triboiontronics with record-high charge density for self-powered sensors and neurologic analogs, Joule 2 (2024) 100332.

[52] R.L.X Li, S. Li, Z.L. Wang, D. Wei, Triboiontronics with temporal control of electrical double layer formation, Nat. Commun. 15 (2024) 6182.

[53] A.B. Alzahraa, M. Eldeeb, J.E. Dick, No microdroplets? No problem. Soap films amplify the interface and produce hydrogen peroxide, J. Am. Chem. Soc. 147 (2025) 3325–33329.

[54] J.M.E.A. McGregor, Organic electrolyte cations promote non-aqueous CO2 reduction by mediating interfacial electric fields, Nat. Catal 8 (2025) 79–91.